Facile synthesis and electrochemical performances of multi-walled carbon nanotubes/poly(3,4-ethylenedioxythiophene) composite films as electrodes for fabric supercapacitors

Yan Chen[1] · Wenyao Yang[2] · Dingyu Yang[1] · Peihua Wangyang[1] · Xu Li[1]

Abstract

In the research of wearable smart electronics, obtaining particular structure electrodes to provide outstanding mechanical flexible and electrochemical performance remains challenging. In this study, flexible multi-walled carbon nanotubes (MWCNTs)/poly(3,4-ethylenedioxythiophene) (PEDOT) nanocomposite electrodes are fabricated via dip-coating and vapor phase polymerization methods. A poriferous network structure of composite electrode is achieved through incorporation of MWCNTs to the conducting polymer matrix. These interconnected holes on electrodes and the synergetic effects between MWCNTs and PEDOT polymer yield large surface areas and favorable electrochemical performances. A single composite electrode exhibits a high areal capacitance of 92.55 F/cm^2, as well as good cycling stability with 94% of its initial charge after 5500 cycles. An all-solid-state micro-supercapacitor based on MWCNTs/PEDOT electrodes is also assembled by sandwiching the polyvinyl alcohol–H_3PO_4 gel electrolyte, which displays an areal capacitance of 32.06 mF/cm^2. This belt-shaped flexible micro-supercapacitor served as energy storage device shows significant potentiality in wearable electronics.

1 Introduction

Flexible supercapacitors have been universally exploited due to their high power density, long cycle life, quick charge–discharge process, low cost as well as mechanical flexible [1, 2]. As an energy storage unit, flexible micro-supercapacitors are also able to be integrated into renewable energy and wearable electronic devices [3, 4]. However, the moderate energy density of flexible supercapacitors limits their application in diverse fields which require high energy throughput [5]. Thus, developing innovative and nanoporous electrode with high mass transportation and large effective surface areas is urgent to realize an enhanced device capacitance. Carbon materials (such as activated carbon, carbon nanotubes, graphene), metal oxide (such as nickel oxide, cobalt oxide, ruthenium oxide, manganese dioxide) and conductive polymers (such as polyaniline, polypyrrole, polythiophene derivative) are three major materials for supercapacitors' electrodes [6–9]. Carbon based materials are attractive due to their high chemical/thermal stability, excellent conductivity and affordable cost, while metal oxides and conducting polymers are extensively used because of their large pseudocapacitance and reversible Faradaic redox capabilities [10, 11]. Among these materials, poly(3,4-ethylenedioxythiophene) (PEDOT) with high thermal stability, high conductivity and easy synthesis is a hopeful material for supercapacitors' electrodes. Moreover, the weak mechanical strength and poor cyclability of PEDOT is able to be mitigated by introducing other materials which possess strong mechanical properties and good cyclic stability to improve the charge storage capacity and extend the cycle life [12]. Multi-walled carbon nanotubes (MWCNTs) possessed of low internal resistance, high mechanical strength together with good stability make them suitable for electrode materials of flexible supercapacitors [13].

The combination of MWCNTs and PEDOT can effectively enhance the capacitive ability of composite electrode to meet energy storage demand. Gao et al. develop an exquisite dynamic three-phase interline electropolymerization to

✉ Dingyu Yang
   yangdingyucuit@163.com

1 Sichuan Province Key Laboratory of Information Materials and Devices Application, College of Optoelectronic Engineering, Chengdu University of Information Technology, Chengdu, People's Republic of China

2 Engineering Research Center of New Energy Storage Devices and Applications, School of Electrical and Electronic Engineering, Chongqing University of Arts and Sciences, Chongqing 402160, People's Republic of China

prepare PEDOT@CNTs composite at a water/oil interface. And the prepared PEDOT@CNTs film shows heterogeneous structures with a capacitance of 0.148 F/C [14]. A co-electrodeposited poly(3,4-ethylenedioxythiophene)/carbon nanotubes–carboxyl graphene (PEDOT/CNT/CG) ternary composite attributed to full use of carboxyl groups distributed on both edges and basal planes of CG sheets displays markedly improved specific capacitance which is as high as 150.6 mF/cm^2 at 0.2 mA/cm^2 [15]. The composite PEDOT coated graphene oxide/carbon nanotubes is fabricated via one-step electrochemical co-deposition and exhibit high areal specific capacitance of 99 mF/cm^2 at 1 mA/cm^2 [16]. In these reports, the combination of conducting polymers and carbon based materials not only presents a synergistic effect, but also forms some typical structures, which play an important role in improving the performances of composites. However, the preparation methods for composite materials mentioned above are complicated and difficult to control. Here, we propose a facile vapor phase polymerization (VPP) process that is controllable and independent of substrate materials to fabricate high performance flexible composite electrodes.

In this study, the MWCNTs/PEDOT hybrid electrodes are fabricated through a two-step process: firstly, the iron p-toluenesulfonate (Fe(OTs)$_3$) oxidant solution contained MWCNTs is dip-coating on the surface of flexible carbon fiber cloth substrate. In the second step, MWCNTs/PEDOT materials are deposited on the textile cloth through VPP process. Unlike the existing electrochemical deposition process, the MWCNTs content in hybrids, the PEDOT molecule arrangement and the morphology formation are able to be regulated in VPP process. The as-prepared hierarchical pore-riched MWCNTs/PEDOT composites with outstanding performances have great potential application in flexible devices.

2 Experimental

A solution of oxidant iron(III) p-toluenesulfonate (Fe(OTs)$_3$) 40 wt% in butanol and MWCNTs (purity: > 95%) were obtained from HC Starck (under the trade names Clevios CB40) and Nanjing XFNANO Materials Tech Co. Ltd, respectively. EDOT (purity: 97%), polyvinyl alcohol (PVA, purity: 98%) and phosphoric acid (H$_3$PO$_4$, purity: 85%) were purchased from Merck (USA).

The preparation process of MWCNTs/PEDOT flexible electrodes was schematically illustrated in Fig. 1. Briefly, the MWCNTs/PEDOT flexible electrodes were prepared via a two-step method: the dip-coating step and the VPP step. Firstly, MWCNTs were dispersed in the oxidant solution which contained Fe(OTs)$_3$ (2 mL) and isopropanol (IPA) (2 mL) by ultrasonic vibration, respectively. Then the carbon
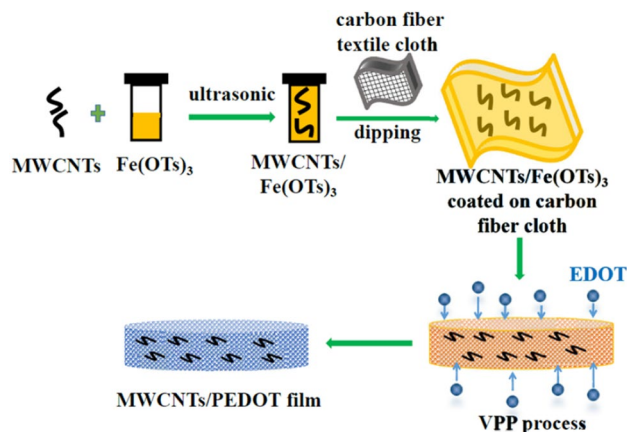

Fig. 1 The preparation process of MWCNTs/PEDOT flexible electrode

fiber textile cloth was dipped into the MWCNTs/Fe(OTs)$_3$ mixed solution for 12 h. During the immersion process, the MWCNTs/Fe(OTs)$_3$ compounds were coated on the surface of textile cloth. Secondly, the dried carbon fiber cloth with MWCNTs/Fe(OTs)$_3$ compounds was exposed to EDOT vapor for complete polymerization. After reaction about 80 min, the obtained carbon fiber textile electrodes were rinsed with ethanol and deionized water several times and denoted as MWCNTs/PEDOT-XX, where XX represents the mass of MWCNTs in the oxidant solution. As comparison, PEDOT textile electrodes without MWCNTs were fabricated by the two-step method as well. The all-solid-state flexible micro-supercapacitors were assembled by placing two textile electrodes of the same size parallel to each other, with PVA–H$_3$PO$_4$ gel as electrolyte and separator. The area of each electrode is 1×1.2 cm^2.

3 Characterization

The crystallographic structures and physical characterizations of as-prepared samples were examined by X-ray diffraction system (XRD, X'Pert Pro MPD), Fourier transform infrared spectrometer (FT-IR, PERKIN ELMER SPECTRUM 400) and Raman spectrometer (Advantage 633 nm). The surface morphology and microstructures of composites were obtained using a scanning electron microscopy (SEM, HITACHI S4800). The capacitance measurements of the electrodes were performed in 1 M H$_2$SO$_4$ aqueous electrolyte in a three-electrode electrochemical cell setup on a CHI660D (Chenhua, Shanghai) electrochemical workstation. Flexible electrodes acted as working electrodes directly. A platinum plate and an Ag/AgCl electrode served as the counter and reference electrode, respectively. The areal capacitances of samples were calculated from the GCD curves based on the

equation: $C_s = (I \times \Delta t)/(S \times \Delta V)$, where C_s is areal capacitance (F/cm^2), I and Δt are charge–discharge current (A) and time (s), respectively, ΔV is the potential drop during discharge (V), and S is the area of the electrode (cm^2). In addition, the electrochemical performances of assembled flexible micro-supercapacitor were examined by standard cyclic voltammetry (CV) and galvanostatic charge–discharge (GCD) techniques.

4 Results and discussion

The crystallographic forms of MWCNTs, PEDOT and MWCNTs/PEDOT (MWCNTs/P) are verified by XRD patterns, as shown in Fig. 2. For pure MWCNTs, the broad diffraction peak at 2θ of ~26° is attributed to the diffraction of (002) lattice plane in graphite [17]. Characteristic peaks of PEDOT are not observed in the spectrum of XRD
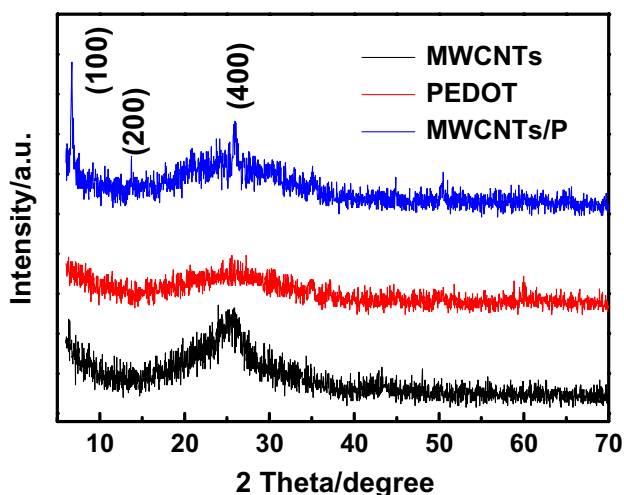
Fig. 2 XRD patterns of MWCNTs, PEDOT and MWCNTs/PEDOT films

pattern, indicating amorphous nature of the polymeric material after VPP. However, three peaks around 6.6°, 11.3° and 25.9° appear in the XRD spectrum of MWCNTs/P composite film. These signals can be readily indexed to the (100), (200) and (400) crystal structure of PEDOT material, which suggests the ordered molecule arrangement of PEDOT in MWCNTs/P composites [18]. Hence, amorphous PEDOT film with dense packing is developed in the VPP process. When the MWCNTs particles are added in the oxidant film, the PEDOT film growth involves production of a loose structure which provides enough space for ordered molecule arrangement, resulting in the crystalline structure formation ultimately.

The chemical structure of electrode films and interaction between MWCNTs and PEDOT are investigated by FT-IR and Raman spectroscopy. FT-IR spectra of PEDOT and MWCNTs/P hybrid film are recorded in Fig. 3a. Distinct peaks belonged to PEDOT are observed in two kinds of films. Peak signals at 567 and 671 cm^{-1} are assigned to oxyethylene ring deformation and C–S–C deformation, respectively. Bands at 832 and 985 cm^{-1} are attributed to C–S vibration in the thiophene ring. Peaks at 1105 and 1209 cm^{-1} are owing to C–O–C bond stretching in the ethylene dioxy group. Besides, C=C and C–C stretching vibrations of the quinonoid structure of thiophene ring are located at 1349 and 1626 cm^{-1} [19–21]. All of the above characteristics peaks are observed in the spectrum of MWCNTs/P composite film in addition to the extra peak at about 1052 cm^{-1} which is attributed to C–O–C stretching vibration [20, 22]. Figure 3b shows the Raman spectra of MWCNTs and MWCNTs/P films. For the Raman spectrum of pristine MWCNTs, two strong peaks located at 1336 cm^{-1} and 1565 cm^{-1} are associated with the amorphous disorder carbon structure (D-band) and the stretching vibration of C–C bond (G-band), respectively [23, 24]. In the Raman spectrum of MWCNTs/P composite film, the bands at 576, 989, 1254, 1364, 1430 and 1505 cm^{-1} correspond to C–O–C bond deformation, oxyethylene ring

Fig. 3 **a** FT-IR spectra of PEDOT and MWCNTs/P; **b** Raman spectra of MWCNTs and MWCNTs/P films
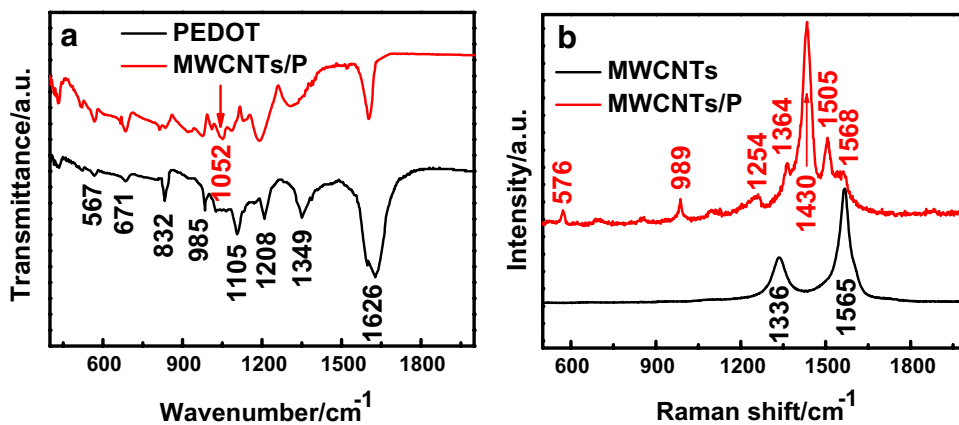
deformation, thiophene C–C inter-ring stretching in plane modes, single C–C stretching, C=C symmetric stretching and C=C antisymmetric stretching in plane modes, respectively [19, 25]. The weak peak at 1568 cm^{-1} belongs to the G band of MWCNTs component. Whereas the G band peak is slightly shifted compared with the G band of pristine MWCNTs, manifesting the formation of strong π-π interaction between PEDOT and MWCNTs [19, 25]. The results above indicate successful fabrication of MWCNTs/P composite film.

Surface morphologies of MWCNTs, PEDOT and MWCNTs/P composite films are characterized by SEM. In Fig. 4a, the micrograph of MWCNTs with the diameter of 10–30 nm presents intertwined fibrillar structure. The VPP PEDOT film in Fig. 4b shows a compact and coarse surface morphology. The surface of MWCNTs/P-5, 7, 10 composite films in Fig. 4c–e changes a lot. Three hybrid films deposited on carbon fiber cloth all display network porous structures, which can increase the surface areas of composite films and facilitate the immersion of the electrolyte and transportation of ions [26]. The additional porous structure of composite films is probably attributed to the modification of MWCNTs during VPP. Whereas, the pores on the surface of composite films enlarges as the amount of carbon nanotubes increasing. This may be due to the agglomeration of partial MWCNTs, which could result in the reduction of the effective use of specific surface area.

The reversibility and electrochemical performances of PEDOT film and its composite film with MWCNTs are analyzed using CV technique. Figure 5a exhibits the CV curves of MWCNTs, PEDOT and MWCNTs/P-7 films under the scan rate of 100 mV/s with a potential range between −0.2 and 1 V (vs Ag/AgCl). Approximately rectangular shapes are observed in CV profiles of MWCNTs and PEDOT films, indicating the significant contribution of electrical double-layer capacitance to the total stored charge [25]. The CV loop of MWCNTs/P-7 hybrid film has larger areas than that of pure MWCNTs and PEDOT films, indicating a better capacitive behavior which can be attributed to the porous structure of composite film and synergetic effect between MWCNTs and PEDOT [20]. Figure 5b displays CV loops of MWCNTs/P-7 composite film at different scan rates from 10 to 100 mV/s. The current density increases proportionally and the CV curves maintain quasi rectangle shape at higher scan rate, implying superior electrochemical reversibility of the composite film [15]. CV curves of MWCNTs/P hybrid films with different amounts of MWCNTs at 100 mV/s are presented in Fig. 5c. It can be seen that the MWCNTs/P-7 hybrid electrode exhibits the highest integration areas, suggesting the highest specific capacitance which results from the suitable amounts of MWCNTs nanoparticles in the hybrid film [27]. Electrochemical impedance spectroscopy (EIS) is a powerful tool to investigate the characteristics of electrode/electrolyte interface [16]. Figure 5d shows the
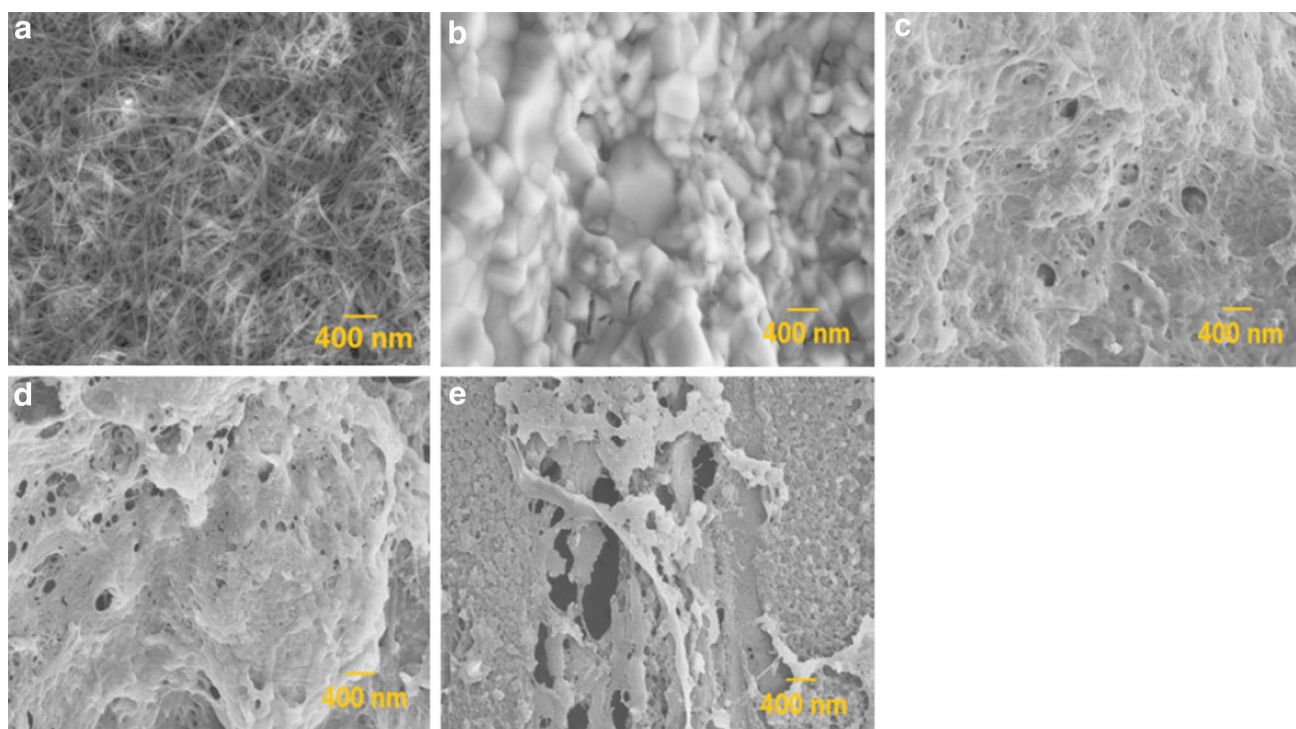

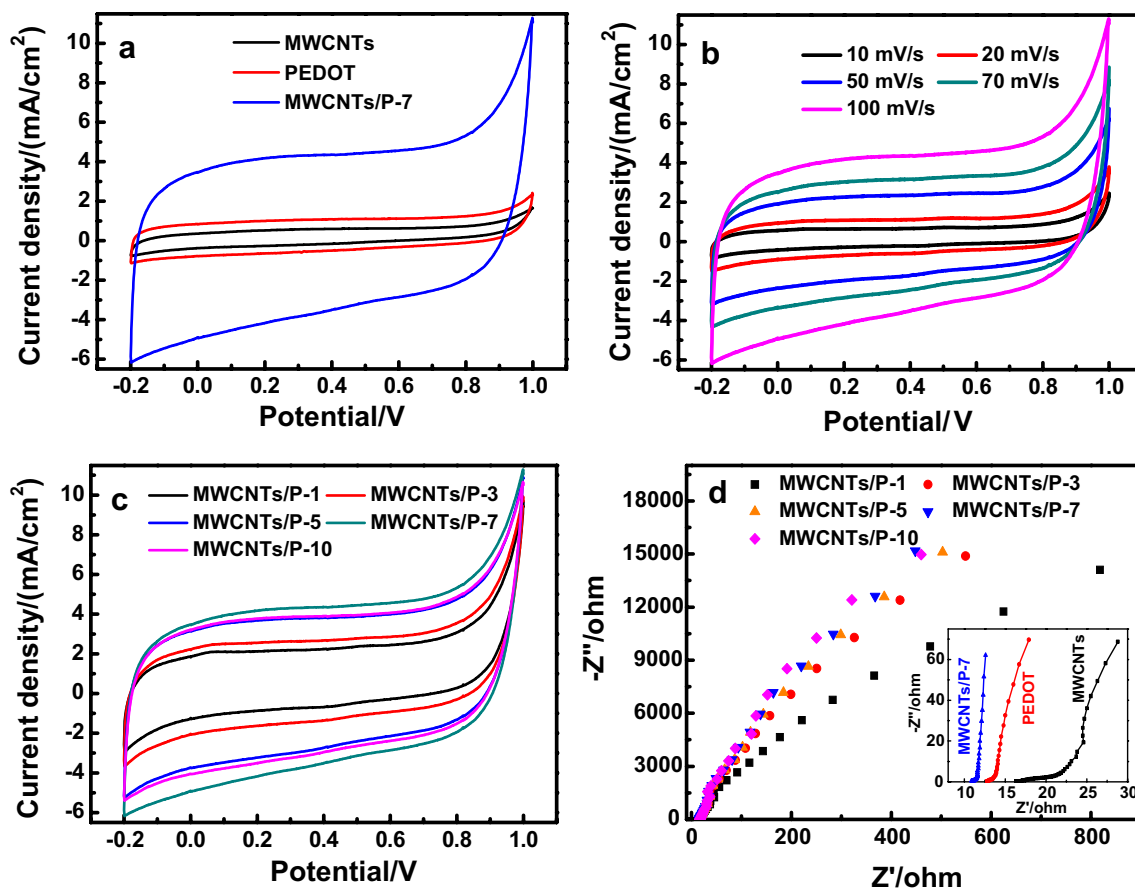**Fig. 4** SEM images of **a** MWCNTs; **b** PEDOT; **c** MWCNTs/P-5; **d** MWCNTs/P-7; **e** MWCNTs/P-10

Fig. 5 a CV curves of MWCNT, PEDOT, MWCNTs/P-7 films; **b** CV curves of MWCNTs/P-7 composite films at different scan rates; **c** CV curves of MWCNTs/P with different MWCNTs loading in films;

d Nyquist plots of impedance data for MWCNTs/P-1,3,5,7,10 films, inset is the Nyquist plots of MWCNTs, PEDOT and MWCNTs/P-7

Nyquist plots of as-prepared samples over the frequency ranges of 0.01 Hz to 100 kHz. The inset exhibits plots of MWCNTs, PEDOT and MWCNTs/P electrodes with enlarged scale. Based on the EIS spectra, the plots of the composite films present almost the same intercept at the real part which can be assigned to the internal resistance (R_s). Besides, the depressed semicircles at high frequency for MWCNTs/P-1, 3, 5, 7, 10 electrodes are observed as well, revealing the low interfacial charge transfer resistance (R_{ct}) [16]. In the inset in Fig. 5d, the R_s values for MWCNTs, PEDOT and MWCNTs/P-7 films are measured to be 16.2, 12.7 and 10.5 Ω, respectively. It is apparent that the addition of MWCNTs can effectively improve the conductive performance of polymer matrix, which results in the lower resistance for MWCNTs/P-7 film. In addition, the low frequency part of the plot for MWCNTs/P-7 films shows more close to 90°, demonstrating an excellent capacitance behavior due to the enhanced porosity of the composite film.

The electrochemical performances of MWCNTs, PEDOT and MWCNTs/P films are further compared by the GCD measurements. Figure 6a exhibits the GCD curves of

MWCNTs, PEDOT and MWCNTs/P-7 electrodes at a current density of 0.3 mA/cm². A nearly symmetrical triangular shape is observed for all GCD curves, which suggests an ideal behavior for supercapacitor [28]. The MWCNTs/P-7 composite film possesses longer discharge time than that of other films, revealing higher capacitance behavior. According to the GCD plots, the value of areal capacitance for MWCNTs/P-7 hybrid film is calculated to be 92.55 mF/cm², which is much higher than that of MWCNTs (3.12 mF/cm²) and PEDOT (11.34 mF/cm²) films. The higher effective surface area of porous structure and better electron transport paths permitted by composite film are responsible for the superior capacitance of hybrid film [16]. Figure 6b shows the GCD polts of MWCNTs/P-7 composite electrode at various current densities. The nearly symmetrical shape is also observed with the current density increasing, demonstrating good electrochemical reversibility and charge–diacharge properties [28]. From the discharge curves in Fig. 6c, the areal capacitances of MWCNTs/P-1, 3, 5, 7, and 10 are 54.58, 64.36, 74.03, 92.55 and 76.93 F/cm², respectively. Obviously, the values of areal capacitance increase with
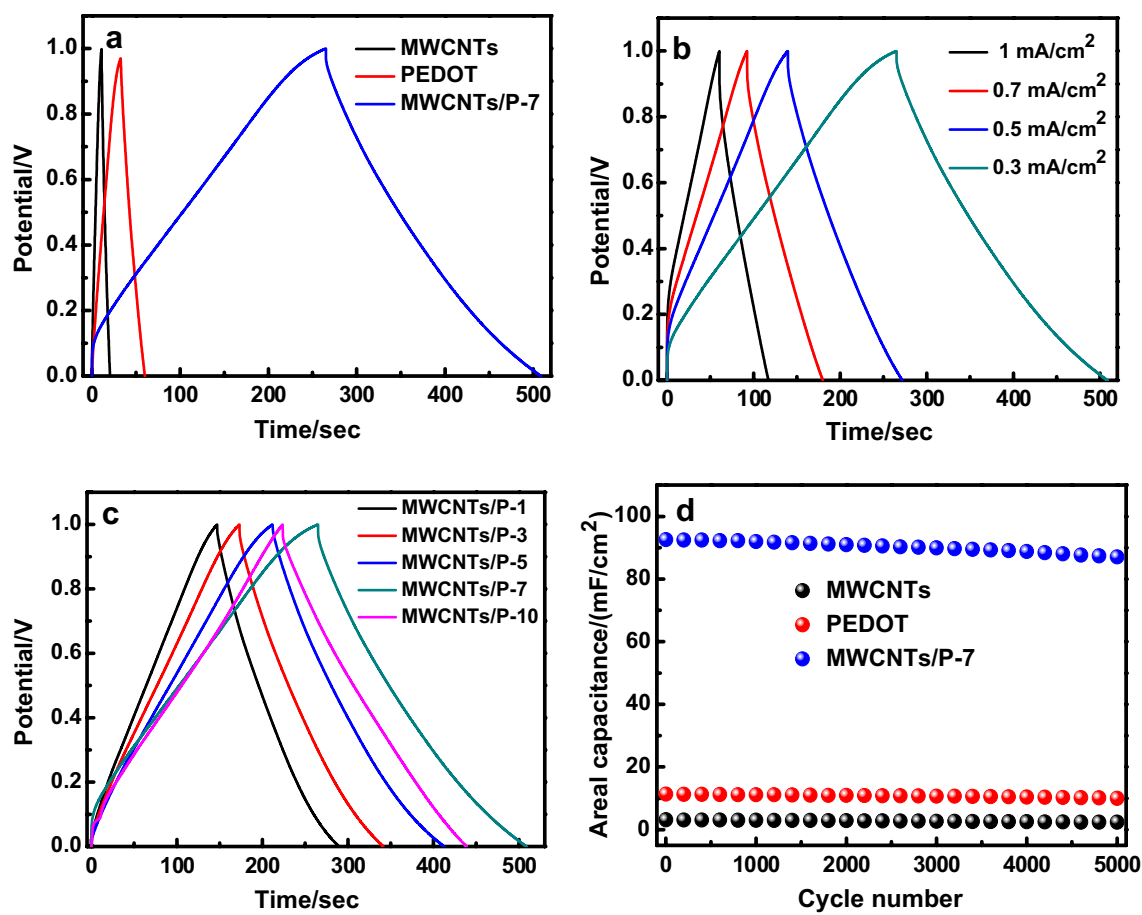
Fig. 6 **a** GCD curves of three kinds of films at a current density of 0.3 mA/cm^2; **b** GCD curves of MWCNTs/P-7 at different current density; **c** charge–discharge curves of MWCNTs/P with different MWCNTs loading; **d** stability plots for three kinds of filmsat a current density of 0.3 mA/cm^2

adding the amount of MWCNTs. The areal capacitance decreases as partial MWCNTs agglomerating. Moreover, the durability of electrodes are investigated using a cyclic GCD test. Figure 6d compares the performance of MWCNTs, PEDOT and MWCNTs/P-7 films over 5500 charge–discharge cycles, with the electrodes showing retention values of 76%, 88% and 94%, respectively. Improved capacitance retention and stability during cycling of MWCNTs/P-7 composite film are attributed to the synergistic effect which can accommodate the stress changes in doping/dedoping process and thus less susceptible to fatigue caused by cycling mechanical stress [29].

The MWCNTs/P composite electrodes are further assembled into strip microsupercapacitor. The poly(vinyl alcohol) (PVA)/H$_3$PO$_4$ gel [30] is used as both solid electrolyte and separator. Figure 7a presents the CV curve of flexible solid-state device with a potential range from − 0.2 to 1 V at a scan rate of 100 mV/s. As can be observed, the CV plot deviates from rectangular shape, which probably indicates poor contact between electrode material and gel electrolyte

[19, 31]. The GCD curve of micro-supercapacitor displayed in Fig. 7b is measured at a current density of 0.1 mA/cm^2. Almost symmetrical isosceles lines demonstrate typical supercapacitive behavior of MWCNTs/P based device. And the areal capacitance of assembled supercapacitor achieves 32.06 mF/cm^2 at a current density of 0.1 mA/cm^2, which provides an insight into the practical application of flexible supercapacitors.

5 Conclusion

A poriferous network structure of MWCNTs/P composite flexible electrode is synthesized via facile VPP method. Synergistic properties and electrochemical behaviour of hybrid film are discussed as well. The as-prepared MWCNTs/P-7 flexible electrode shows a high areal capacitance of 92.55 mF/cm^2 at a current density of 0.3 mA/cm^2 and excellent long-term cyclability. Based on PVA/H$_3$PO$_4$ gel electrolyte, the assembled flexible microdevice exhibits

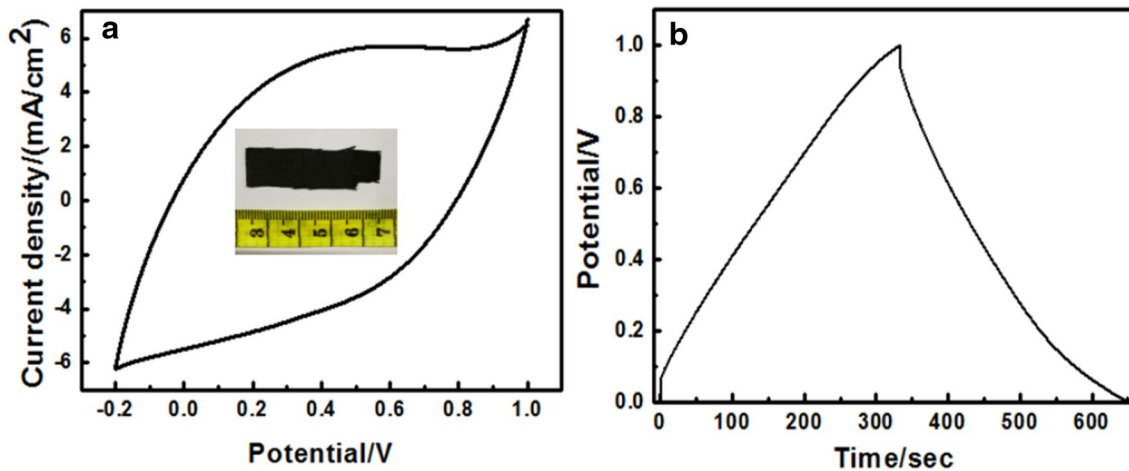**Fig. 7** **a** CV curve of solid-state device at a scan rate of 100 mV/s; **b** GCD curve of the assembled device at a current density of 0.1 mA/cm^2

an areal capacitance of 32.06 mF/cm^2 at a current density of 0.1 mA/cm^2, which provides an insight into the practical application of flexible supercapacitors.

References

1. X. Wang, X. Lu, B. Liu, D. Chen, Y. Tong, G. Shen, Flexible energy-storage devices: design consideration and recent progress. Adv. Mater. **26**, 4763–4782 (2014)
2. B. Yao, J. Zhang, T. Kou, Y. Song, T. Liu, Y. Li, Paper-based electrodes for flexible energy storage devices. Adv. Sci. **4**, 1700107 (2017)
3. P. Simon, Y. Gogotsi, Materials for electrochemical capacitors. Nat. Mater. **7**, 845–854 (2008)
4. X. Zhao, B.M. Sánchez, P.J. Dobson, P.S. Grant, The role of nanomaterials in redox-based supercapacitors for next generation energy storage devices. Nanoscale **3**, 839–855 (2011)
5. W. Raza, F. Ali, N. Raza, Y.W. Luo, E.E. Kwon, J.H. Yang, S. Kumar, A. Mehmood, E.E. Kwon, Recent advancements in supercapacitor technology. Nano Energy **52**, 441–473 (2018)
6. K.S. Ryu, K.M. Kim, N.G. Park, Y.J. Park, S.H. Chang, Symmetric redox supercapacitor with conducting polyaniline electrodes. J. Power Sources **103**, 305–309 (2002)
7. Y. Wang, J. Guo, T. Wang, J. Shao, D. Wang, Y.W. Yang, Mesoporous transition metal oxides for supercapacitors. Nanomaterials **5**, 1667–1689 (2015)
8. M. Cakici, R.R. Kakarla, F. Alonso-Marroquin, Advanced electrochemical energy storage supercapacitors based on the flexible carbon fiber fabric-coated with uniform coral-like MnO$_2$ structured electrodes. Chem. Eng. J. **309**, 151–158 (2017)
9. S. Ahmed, M. Rafat, Hydrothermal synthesis of PEDOT/rGO composite for supercapacitor application. Mater. Res. Express **5**, 015507 (2018)
10. S.S. Jayaseelan, S. Radhakrishnan, B. Saravanakumar, M.-K. Seo, M.-S. Khil, H.-Y. Kim, M.-S. Khil, H.-Y. Kim, B.-S. Kim, Mesoporous 3D NiCo$_2$O$_4$/MWCNT nanocomposite aerogels prepared by a supercritical CO$_2$ drying method for high performance hybrid supercapacitor electrodes. Colloids Surf. A **538**, 451–459 (2018)
11. S. Ahmed, M. Rafat, M.K. Singh, S.A. Hashmi, Free-standing, flexible PEDOT-PSS film and its nanocomposites with graphene nano-platelets as electrodes for quasi-solid-state supercapacitors. Nanotechnology **29**, 395401 (2018)
12. Q. Meng, K. Cai, Y. Chen, L. Chen, Research progress on conducting polymer based supercapacitor electrode materials. Nano Energy **36**, 268–285 (2017)
13. K. Koziol, J. Vilatela, A. Moisala, M. Motta, P. Cunniff, M. Sennett, A. Windle, Highperformance carbon nanotube fiber. Science **318**, 1892–1895 (2007)
14. L.L. Gao, X.H. Mao, H. Zhu, W. Xiao, F.X. Gan, D.H. Wang, Electropolymerization of PEDOT on CNTs conductive network assembled at water/oil interface. Electrochim. Acta **136**, 97–104 (2016)
15. H.H. Zhou, X.M. Zhi, Ternary composite electrodes based on poly(3,4-ethylenedioxythiophene)/carbon nanotubes-carboxyl graphene for improved electrochemical capacitive performances. Synth. Met. **234**, 139–144 (2017)
16. H.H. Zhou, G.Y. Han, One-step fabrication of heterogeneous conducting polymers-coated graphene oxide/carbon nanotubes composite films for high-performance supercapacitors. Electrochim. Acta **192**, 448–455 (2016)
17. G.X. Huang, Y. Zhang, L. Wang, P. Sheng, H.S. Peng, Fiber-based MnO$_2$/carbon nanotube/polyimide asymmetric supercapacitor. Carbon **125**, 595–604 (2017)
18. L. Niu, C. Kvarnström, K. Fröberg, A. Ivaska, Electrochemically controlled surface morphology and crystallinity in poly(3,4-ethylenedioxythiophene) films. Synth. Met. **122**, 425–429 (2001)
19. A.K. Thakur, A.B. Deshmukh, R.B. Choudhary, I. Karbhal, M. Majumder, M.V. Shelke, Facile synthesis and electrochemical evaluation of PANI/CNT/MoS$_2$ ternary composite as an electrode material for high performance supercapacitor. Meter. Sci. Eng. B **223**, 24–34 (2017)

20. Z. Chen, X. Meng, S. Wang, J. Wang, J.M. Liu, R. Xue., H. Ma, H. Dong, H.B. Yu, PEDOT:PSS-MWCNTs modified carbon black-based gas diffusion electrodes for improved performance of in-situ electrocatalytic flue gas desulfurization. J. Clean. Prod. **200**, 1087–1099 (2018)

21. S. Deshagani, K. Krushnamurty, M. Deepa, High energy density, robust and economical supercapacitor with poly(3,4-ethylenedioxythiophene)-CO_2 activated rice husk derived carbon hybrid electrodes. Mater. Energy **9**, 137–153 (2018)

22. Y. Chen, J.H. Xu, Y.J. Yang, Y.T. Zhao, W.Y. Yang, X. He, S.B. Li, C.Y. Jia, Enhanced electrochemical performance of laser scribed graphene films decorated with manganese dioxide nanoparticles. J. Mater. Sci.: Mater. Electron. **27**, 2564–2573 (2016)

23. A. Aydinli, R. Yuksel, H.E. Unalan, Vertically aligned carbon nanotube-polyaniline nanocomposite supercapacitor electrodes. Int. J. Hydrogen Energy **43**, 18617–18625 (2018)

24. J. Garcia-Torres, C. Crean, Ternary composite solid-state flexible supercapacitor based on nanocarbons/manganese dioxide/PEDOT:PSS fibres. Mater. Des. **155**, 194–202 (2018)

25. Y. Chen, J.H. Xu, Y.J. Yang, S.B. Li, W.Y. Yang, T.J. Peng, X.L. Mao, Y.T. Zhao, PEDOT:PSS/graphene/PEDOT ternary film for high performance electrochemical electrode. J. Mater. Sci.: Mater. Electron. **26**, 8292–8300 (2015)

26. N. Wang, G.Y. Han, H. Song, Y.M. Xiao, Y.P. Li, Y. Zhang, H.F. Wang, Integrated flexible supercapacitor based on poly(3,4-ethylenedioxythiophene) deposited on Au/porous polypropylene film/Au. J. Power Source **395**, 228–236 (2018)

27. J. He, D. Yang, H. Li, X. Cao, L.P. Kang, X.X. He, R.B. Jiang, J. Sun, Z.B. Lei, Z.-H. Liu, Mn_3O_4/RGO/SWCNT hybrid film for all-solid-state flexible supercapacitor with high energy density. Electrochim. Acta **283**, 174–182 (2018)

28. S.N.J.S.Z. Abidin, M.S. Mamat, S.A. Rasyid, Z. Zainal, Y. Sulaiman, Electropolymerization of poly(3,4-ethylenedioxythiophene) onto polyvinyl alcohol-graphene quantum dot-cobalt oxide nanofiber composite for high-performance supercapacitor. Electrochim. Acta **261**, 548–556 (2018)

29. J. Xu, J.N. Ding, X.S. Zhou, Y. Zhang, W.J. Zhu, Z.F. Liu, S.H. Ge, N.Y. Yuan, S.L. Fang, R.H. Baughman, Enhanced rate performance of flexible and stretchable linear supercapacitors based on polyaniline@Au@carbon nanotube with ultrafast axial electron transport. J. power Source **340**, 302–308 (2017)

30. X. Xiao, T.Q. Li, P.H. Yang, Y. Gao, H.Y. Jin, W.J. Ni, W.H. Zhan, X.H. Zhang, Y.Z. Cao, J.W. Zhong, L. Gong, W.-C. Yen, W.J. Mai, J. Chen, K.F. Hou, Y.-L. Chueh, Z.L. Wang, H. Zhou, Fiber-based all-solidstate flexible supercapacitors for self-powered systems. ACS Nano **6**, 9200–9206 (2012)

31. A.Q. Liang, D.Q. Li, W.Q. Zhou, Y.L. Wu, G. Ye, J. Wu, Y.N. Chang, R. Wang, J.K. Xu, G.M. Nie, J. Hou, Y.K. Du, Robust flexible WS_2/PEDOT:PSS film for use in high-performance miniature supercapacitor. J. Electroanal. Chem. **824**, 136–146 (2018)